The FOXO Transcription Factor DAF-16 Bypasses *ire-1* Requirement to Promote Endoplasmic Reticulum Homeostasis

Modi Safra,[1] Rolf Fickentscher,[2] Mor Levi-Ferber,[1] Yehuda M. Danino,[1] Anat Haviv-Chesner,[1] Malene Hansen,[3] Tamar Juven-Gershon,[1] Matthias Weiss,[2] and Sivan Henis-Korenblit[1,*]
[1]The Mina and Everard Goodman Faculty of Life Sciences, Bar-Ilan University, 5290002 Ramat Gan, Israel
[2]Experimental Physics I, University of Bayreuth, 95440 Bayreuth, Germany
[3]Program of Development, Aging and Regeneration, Sanford-Burnham Medical Research Institute, La Jolla, CA 92037, USA
*Correspondence: sivan.korenblit@biu.ac.il
http://dx.doi.org/10.1016/j.cmet.2014.09.006

SUMMARY

The unfolded protein response (UPR) allows cells to adjust the capacity of the endoplasmic reticulum (ER) to the load of ER-associated tasks. We show that activation of the *Caenorhabditis elegans* transcription factor DAF-16 and its human homolog FOXO3 restore secretory protein metabolism when the UPR is dysfunctional. We show that DAF-16 establishes alternative ER-associated degradation systems that degrade misfolded proteins independently of the ER stress sensor *ire-1* and the ER-associated E3 ubiquitin ligase complex *sel-11/sel-1*. This is achieved by enabling autophagy-mediated degradation and by increasing the levels of *skr-5*, a component of an ER-associated ubiquitin ligase complex. These degradation systems can act together with the conserved UPR to improve ER homeostasis and ER stress resistance, beyond wild-type levels. Because there is no sensor in the ER that activates DAF-16 in response to intrinsic ER stress, natural or artificial interventions that activate DAF-16 may be useful therapeutic approaches to maintain ER homeostasis.

INTRODUCTION

The endoplasmic reticulum (ER) is the site where secretory proteins mature and fold. Misfolded proteins in the ER are refolded by ER resident chaperones or marked for degradation. The latter are retranslocated to the cytosol, ubiquitinated by the *Hrd1/Hrd3* E3 ubiquitin ligase complex, and cleared by a proteasome-mediated form of ER-associated degradation (ERAD) (Smith et al., 2011). In some cases, terminally misfolded proteins are cleared from the ER through ERAD(II), an autophagy-mediated form of ERAD (Fujita et al., 2007).

Accumulation of misfolded proteins in the ER triggers the unfolded protein response (UPR). The UPR coordinates processes that decrease translation and increase the levels of ER-resident chaperones and of ERAD components (Ron and Walter, 2007) to restore ER homeostasis. In *Caenorhabditis elegans*, three proteins sense ER stress and activate the UPR: the

PERK kinase homolog PEK-1, the transcription factor ATF-6, and the ribonuclease inositol-requiring protein-1 (IRE-1). Upon ER stress, activated IRE-1 removes an intron from *xbp-1* (X-box binding protein-1) mRNA through unconventional splicing. The spliced version of the XBP-1 transcription factor regulates the expression of many UPR genes, including genes that encode ER resident chaperones and genes involved in ERAD (Calfon et al., 2002; Shen et al., 2001, 2005; Urano et al., 2002).

C. elegans daf-2 insulin/IGF-1 signaling (IIS) mutants are resistant to ER stress, yet their IRE-1 and XBP-1 activities are relatively reduced (Henis-Korenblit et al., 2010). This may indicate that ER homeostasis is improved in *daf-2* mutants independently of *xbp-1* activation.

Here, we investigated how reduced IIS improves ER homeostasis and ER stress resistance in *C. elegans*. We find that the IIS-regulated transcription factor DAF-16 establishes parallel protein degradation systems for removal and elimination of misfolded secretory proteins from the ER. These systems can replace the canonical protein degradation pathways when the *ire-1* UPR pathway is blocked, and generate enhanced ER stress resistance when both the canonical UPR pathways and the *daf-16*-induced pathways are intact.

RESULTS

Reduced IIS Maintains ER Homeostasis Independently of *xbp-1*

Previous studies showed that *xbp-1* splicing is increased in *xbp-1(zc12)* mutants compared to wild-type animals, probably reflecting inefficient maintenance of ER homeostasis in animals with a defective UPR. (The *zc12* allele contains a point mutation that generates a premature stop codon, without destroying the *ire-1* splicing site; Richardson et al., 2011; Safra et al., 2013). We examined the level of *xbp-1* splicing in *daf-2 xbp-1* double mutants and found it to be as low as in *daf-2* single mutants (Figure 1A). Assuming that the activation of the UPR arms correlates with the need to overcome an imbalance in ER homeostasis, these findings suggest that *daf-2* mutations allow the maintenance of ER homeostasis independently of *xbp-1*.

Reduced IIS Improves Tunicamycin Resistance Independently of *xbp-1* and *ire-1*

If reducing IIS improves ER homeostasis in *xbp-1* mutants, their tolerance for ER stress should be improved as well. However,
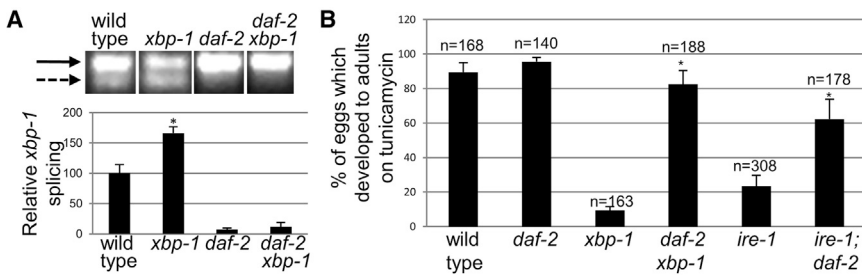
Figure 1. *daf-2* Mutation Improves ER Homeostasis Independently of *xbp-1*

(A) RT-PCR of *xbp-1* transcripts in day 1 animals using primers encompassing the *ire-1*-spliced intron. Top: representative steady-state RT-PCR of unspliced (solid arrow) and *ire-1*-spliced (dashed arrow) *xbp-1* transcripts. Bar graph shows the normalized mean ratio ± SEM of spliced/unspliced *xbp-1* transcripts in three independent biological experiments. The *xbp-1(zc12)* mutation significantly increased *xbp-1* splicing in otherwise wild-type animals ($p < 0.01$), but not in *daf-2* mutants ($p = 0.29$).

(B) Eggs from wild-type, *daf-2(e1370)*, *xbp-1(tm2457)*, *daf-2(e1370) xbp-1(tm2457)*, *ire-1(ok799)* and *ire-1(ok799); daf-2(e1370)* animals were exposed to 1 μg/ml tunicamycin. Percentage of eggs ± SEM that developed into mature L4 or adults within 4 days is shown. Each strain was scored in at least three independent experiments. "n" indicates number of eggs analyzed. Asterisks mark Student's t test values of $p < 0.005$ of *daf-2(−)* compared to *daf-2(+)* animals. See also Figure S2.

daf-2 xbp-1 double mutants are as sensitive to 5 μg/ml tunicamycin as *xbp-1* single mutants (Henis-Korenblit et al., 2010). To test this more thoroughly, eggs of different genotypes were treated with a wider range of tunicamycin concentrations, and their development into adults was assessed. As before, *xbp-1* and *ire-1* single mutants and *daf-2 xbp-1* and *ire-1; daf-2* double mutants were all sensitive to 5 μg/ml tunicamycin, whereas *daf-2* single mutants were relatively resistant (data not shown). However, the *daf-2* mutation did improve the ER stress resistance of *xbp-1/ire-1*-deficient animal when treated with low tunicamycin concentrations, which were compatible with the development of wild-type animals but were incompatible with the development of *xbp-1* or *ire-1* mutants (Figure 1B). Thus, reducing IIS significantly improves ER stress resistance in the absence of *ire-1/xbp-1* under limited ER stress conditions, but not under extreme ER stress conditions.

Reducing IIS Improves Protein Secretion in *ire-1/xbp-1*-Deficient Animals

In *C. elegans*, the *ire-1/xbp-1* ER stress response pathway is required for efficient production and secretion of DAF-28::GFP, a fluorescently-labeled insulin (Safra et al., 2013; Safra and Henis-Korenblit, 2014). Thus, we examined how reducing IIS affects the production and secretion of DAF-28::GFP. Because coelomocytes are dysfunctional in *ire-1/xbp-1* mutants (Safra et al., 2013), we assessed DAF-28::GFP secretion by its levels in the body cavity of animals whose coelomocyte function has been deliberately disrupted by a *cup-4* mutation (Patton et al., 2005). Whereas *xbp-1* mutants did not accumulate fluorescent DAF-28::GFP in their body cavity, secreted fluorescent protein did accumulate in the body cavities of *daf-2 xbp-1* coelomocyte-defective mutants (Figures 2A and 2B). A similar DAF-28::GFP expression pattern was observed by immunostaining with anti-GFP antibodies (Figure S1A and S1B available online), confirming that the differential detection of DAF-28::GFP fluorescence in the body cavity reflects its expression pattern rather than its ability to fluoresce. Reducing IIS improved DAF-28::GFP secretion independently of *pek-1* or *atf-6* (Figure S1C) and was maintained even in the presence of tunicamycin (Figure S1D).

In the absence of *xbp-1/ire-1*, DAF-28::GFP accumulates in the ER of its producing cells, the ASI/ASJ neurons and the posterior intestine (Safra et al., 2013). Reducing IIS decreased the levels of DAF-28::GFP fluorescence in the DAF-28::GFP-producing cells in the hindgut of *xbp-1* and *ire-1* mutants (Figures 2A, 2C, and 2E). In contrast, the high fluorescence levels of

DAF-28::GFP in the ASI/ASJ neurons persisted in *ire-1; daf-2* and *daf-2 xbp-1* double mutants (Figures 2A, 2C, and 2D). A similar effect on DAF-28::GFP expression levels in the producing cells was observed by immunostaining with anti-GFP antibodies (Figure S1B). These findings could be accounted for by an improvement in protein secretion in *xbp-1/ire-1*-deficient intestinal cells upon reduction of IIS.

Coelomocytes Are Functional in *daf-2 xbp-1* Double Mutants, but Not in *ire-1; daf-2* Double Mutants

Although coelomocyte cells are present in *ire-1* and *xbp-1* mutants, they do not internalize material from the body cavity (Safra et al., 2013). Two lines of evidence suggest that this is a result of dysfunctional coelomocytes rather than simply a consequence of a secretory defect: (1) fluorescent material can be detected in the coelomocytes of *ire-1* mutants upon restoration of coelomocyte function by coelomocyte-specific expression of IRE-1, in spite of their severe secretory defects (Safra et al., 2013). (2) Even when secreted fluorescent material is detected in the body cavity of *xbp-1* mutants, it is not detected in their coelomocytes (Figure S1E).

After establishing that *daf-2* mutations restore protein secretion in *ire-1/xbp-1* mutants, we examined whether functional fluorescent coelomocytes could be detected in *daf-2 xbp-1* double mutants expressing DAF-28::GFP. Indeed, fluorescent coelomocytes were detected in some of the *daf-2 xbp-1* double mutants, but not in any of the *xbp-1* single mutants examined (Figure S1F). Furthermore, inactivation of *cup-4* to deliberately interfere with coelomocyte function significantly increased the fluorescence levels in the body cavity of *daf-2 xbp-1* double mutants expressing secreted fluorescent transgenic proteins (Figures 2A, 2B, and S1G). This implied that the low levels of secreted reporters in the body cavity of *daf-2 xbp-1* double mutants are primarily due to their clearance by functional coelomocytes.

Similarly, we examined the effect of *daf-2* mutation on the expression pattern of the secreted reporters in *ire-1*-deficient animals. We found that the fluorescence of DAF-28::GFP and of muscle-derived ssGFP in the body cavities of *ire-1* mutants was increased in a *daf-2(−)* background (Figures 2C and 2D), as expected in animals with functional secretion but with dysfunctional coelomocytes. Furthermore, fluorescent material was detected surrounding the coelomocytes in *ire-1; daf-2* double mutants expressing the DAF-28::GFP transgene, and not within them (Figure S1H).
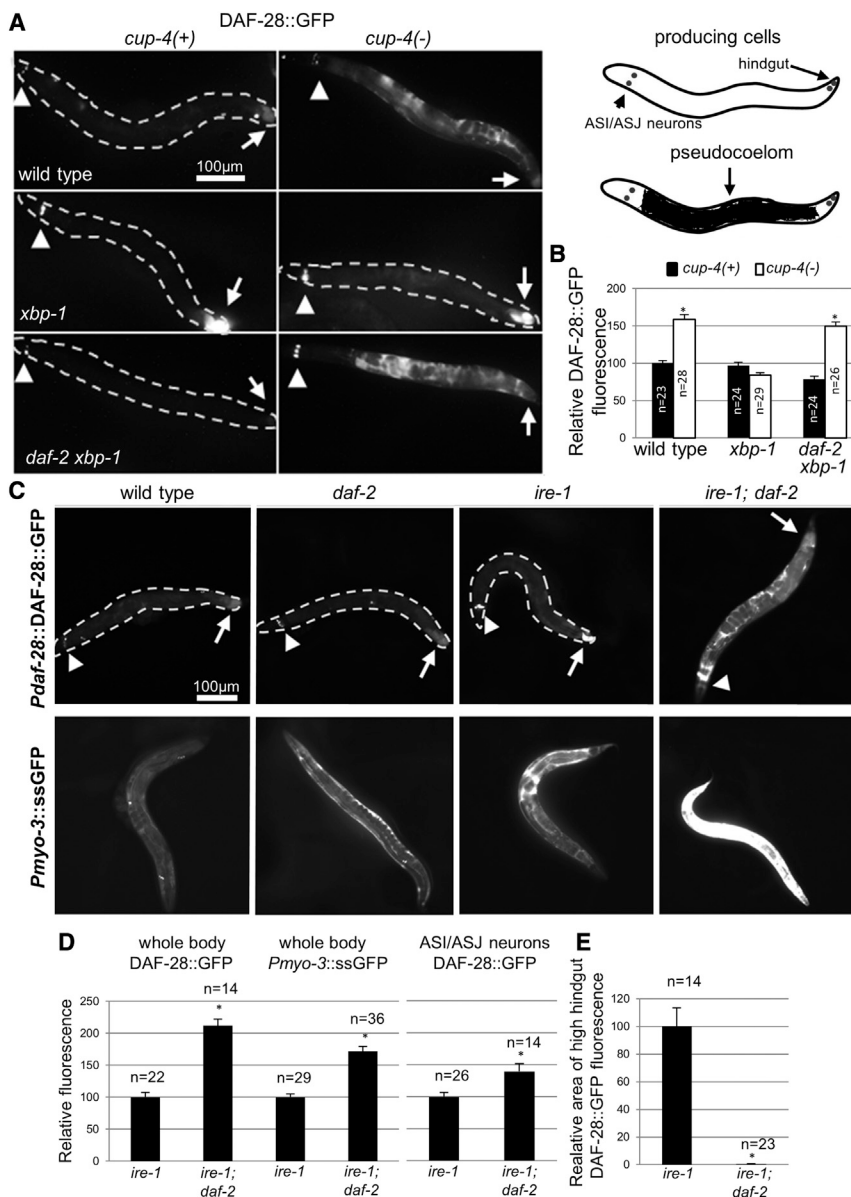
CellPress

Figure 2. *daf-2* Deficiency Restores Protein Secretion in *ire-1* and *xbp-1* Mutants

(A and B) Coelomocyte inactivation by a *cup-4* mutation increased DAF-28::GFP fluorescence in the body cavities of wild-type animals and in *daf-2 xbp-1* double mutants, indicating that DAF-28::GFP secretion and coelomocytes were both functional in these backgrounds. Representative fluorescence micrographs of day 2 adults expressing the DAF-28::GFP transgene (A). Bar graph presents normalized mean ratio ± SEM of whole body DAF-28::GFP fluorescence of day 2 animals (B). Similar results were obtained in two additional independent experiments. Asterisks mark Student's t test values of p < 0.0001 of *cup-4(−)* compared to *cup-4(+)* animals.

(C) Representative fluorescence micrographs of day 3 adults expressing a integrated DAF-28::GFP transgene (upper) or day 1 adults expressing a *Pmyo-3*::ssGFP transgene (lower).

(D) Mean ratio ± SEM of DAF-28::GFP or *Pmyo-3*::ssGFP fluorescence in the whole body or in the ASI/ASJ neurons normalized to the corresponding fluorescence in *ire-1* single mutants.

(E) Mean ratio ± SEM of DAF-28::GFP fluorescent hindgut area in *ire-1; daf-2* double mutants compared to that of *ire-1* single mutants. Area was determined by setting a fluorescence threshold that excluded the fluorescence of other areas of the animal. Asterisks mark Student's t test values of p < 0.01 of *ire-1; daf-2* double mutants compared to *ire-1* single mutant. "n" indicates number of animals analyzed. Similar results were obtained in three independent experiments. Full arrows mark hindgut and arrowheads mark ASI/ASJ neurons as indicated in the schematic representation.

See also Figure S1.

Reduced IIS Improves the Degradation of Misfolded Lumenal Proteins in *ire-1* Mutants

We examined how reducing IIS in *ire-1*-deficient animals affected the levels of a *Pdaf-28*::GFP transcriptional reporter and a *Pdaf-28*::DAF-28::GFP translational reporter. Reducing IIS did not alter the fluorescence of a *daf-28* transcriptional reporter (Figure 3C). At the same time, reducing IIS in *ire-1* mutants increased the overall fluorescence of the DAF-28::GFP translational reporter (Figure 3B) and decreased DAF-28::GFP total protein levels detected by western blotting (Figure 3A). Because western blotting detects DAF-28::GFP irrespective of its folding state and assuming that misfolded DAF-28::GFP does not fluoresce as well as properly folded DAF-28::GFP, this may indicate that reducing IIS improves DAF-28::GFP folding and decreases the levels of misfolded DAF-28::GFP in *ire-1*-deficient animals. This interpretation is consistent with the improved secretion of DAF-28::GFP in *daf-2 xbp-1 cup-4* mutants compared to *xbp-1 cup-4* mutants, as observed by immunofluorescence (Figures S1A and S1B).

Inactivation of ERAD, which leads to the accumulation of DAF-28::GFP intended for degradation, also increases DAF-28::GFP
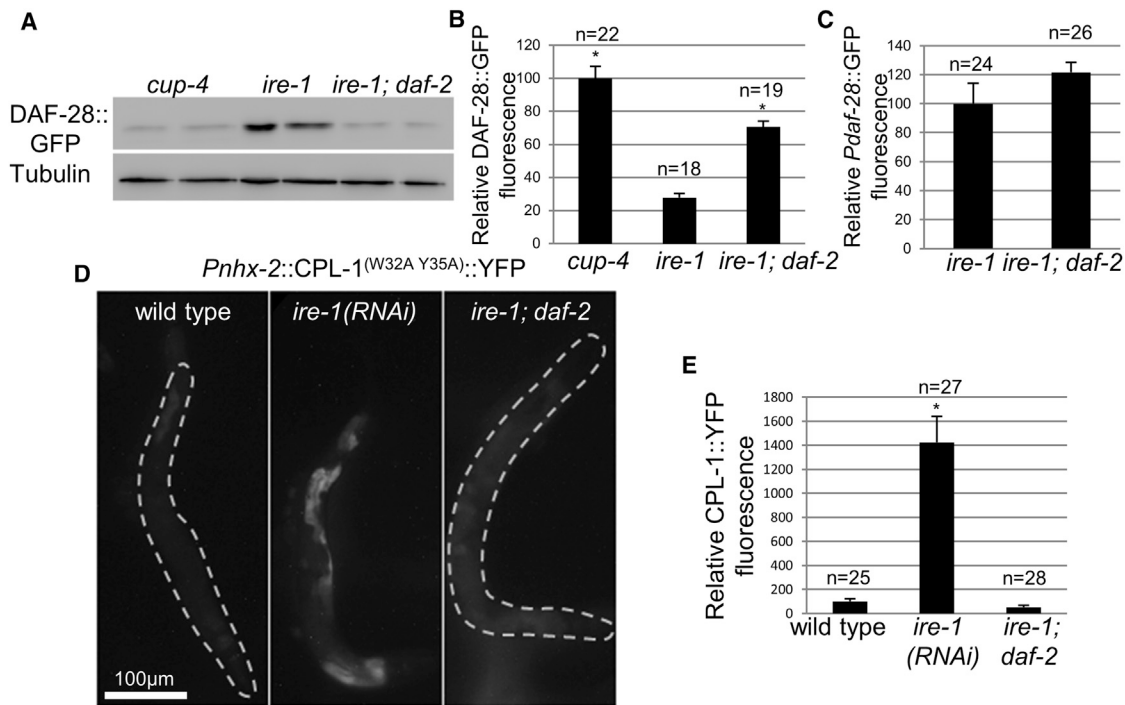
We conclude that reducing IIS restores protein internalization by coelomocytes in *xbp-1*-deficient animals, but not in *ire-1*-deficient animals. This discrepancy may be due to the severity of ER stress associated with *ire-1* deficiency compared to the *xbp-1* deficiency (Safra et al., 2013). Accordingly, although reducing IIS compensates for the deficiency in *ire-1* or *xbp-1* upon exposure to low doses of tunicamycin (Figure 1B), it cannot compensate for their deficiency under harsher ER stress conditions of high concentrations of tunicamycin (Henis-Korenblit et al., 2010). Alternatively, this discrepancy may be due to *xbp-1*-independent functions of *ire-1* that are not bypassed when IIS is reduced. Specifically, we considered the possibility that IRE-1-mediated activation of JNK may act together with IIS to affect ER homeostasis (Oh et al., 2005; Urano et al., 2000). However, this scenario was ruled out because *jnk-1*-related genes did not contribute to the ER stress resistance of *daf-2* mutants (Figure S2).

Figure 3. *daf-2* **Deficiency Reduces the Levels of Misfolded Secretory Proteins in** *ire-1* **Mutants**

(A–C) The levels of a *daf-28* translational reporter (A and B) and a *daf-28* transcriptional reporter (C) were determined in day 2 animals by western blotting (A) and by whole-body fluorescence measurements ± SEM (B and C). Asterisks mark Student's t test values of p < 0.01 compared to *ire-1* single mutants.

(D) Representative fluorescence micrographs of day 1 animals expressing a *Pnhx-2*::CPL-1 (W32A Y35A)::YFP transgene and treated with control or *ire-1* RNAi.

(E) Normalized mean CPL-1 (W32A Y35A)::YFP fluorescence measurements ± SEM of the corresponding *Pnhx-2*::CPL-1 (W32A Y35A)::YFP transgenic animals. All experiments were repeated at least three independent times. "n" indicates number of animals analyzed.

levels detected by western blotting without affecting DAF-28::GFP fluorescence (Safra et al., 2013). Thus, it is possible that the decrease in the level of nonfluorescent DAF-28::GFP protein in *ire-1; daf-2* double mutants may be due to restored ERAD function in these animals. To directly explore ERAD function in *ire-1; daf-2* double mutants, we used a transgenic line expressing mutated CPL-1::YFP (W35A and Y35A) in the intestine. Unlike DAF-28::GFP, whose fluorescence does not increase upon ERAD inactivation, both protein levels and fluorescence of mutated CPL-1::YFP increase upon ERAD inactivation (Miedel et al., 2012). In animals with a functional ERAD, mutated CPL-1::YFP is efficiently degraded, resulting in a low fluorescence signal (Miedel et al., 2012). Consistent with the ERAD pathway being dysfunctional in *ire-1*-deficient animals, *ire-1* RNAi treatment increased CPL-1::YFP fluorescence in the intestine (Figures 3D and 3E). Our attempts to introduce an *ire-1* mutation into the mutant CPL-1::YFP transgenic animals failed, probably due to the sensitivity of *ire-1* mutants to the overexpression of this misfolded protein. However, we successfully generated *ire-1; daf-2* double mutants expressing the mutated CPL-1::YFP transgene, implying that *ire-1* deficient animals can tolerate the expression of the misfolded lysosomal protein once IIS was reduced. Accordingly, *ire-1; daf-2* double mutants did not accumulate mutated CPL-1::YFP (Figures 3D and 3E). These further suggest that ERAD function may be restored in *ire-1; daf-2* double mutants.

Misfolded Lumenal Proteins Are Degraded Independently of the *sel-11/sel-1* E3 Ubiquitin Ligase Complex when IIS Is Reduced

Does reducing IIS restore the same ERAD pathway that is utilized in wild-type animals? To address this, we treated wild-type animals and *daf-2* mutants expressing mutated CPL-1::YFP with RNAi targeting key ERAD components, essential for the clearance of misfolded secretory proteins in wild-type animals. We found that inactivation of the ER-localized α-mannosidase-like gene *edem-1* increased mutated CPL-1::YFP fluorescence both in wild-type animals and in *daf-2* mutants (Figure 4A). Because the only known function of EDEM-1 is the release of terminally misfolded proteins from the calnexin chaperone system by mannose-trimming (Molinari et al., 2003), this implies that *edem-1*-mediated release of misfolded proteins from the ER refolding cycle is a prerequisite for their degradation in *daf-2* mutants as well.

The E3 ubiquitin ligase *Hrd1/sel-11* and the substrate receptor *Hrd3/sel-1* are core components of a large multisubunit ER-embedded ubiquitin ligase complex that tags misfolded proteins from the ER lumen with ubiquitin as they are retrotranslocated out of the ER (Kikkert et al., 2004). *cup-2* (a Der1 homolog) is another stoichiometric subunit of this complex, whose yeast homolog promotes the insertion misfolded proteins into the ER membrane, as they are translocated into the cytosol (Knop et al., 1996; Mehnert et al., 2014). RNAi inactivation of *sel-1*,
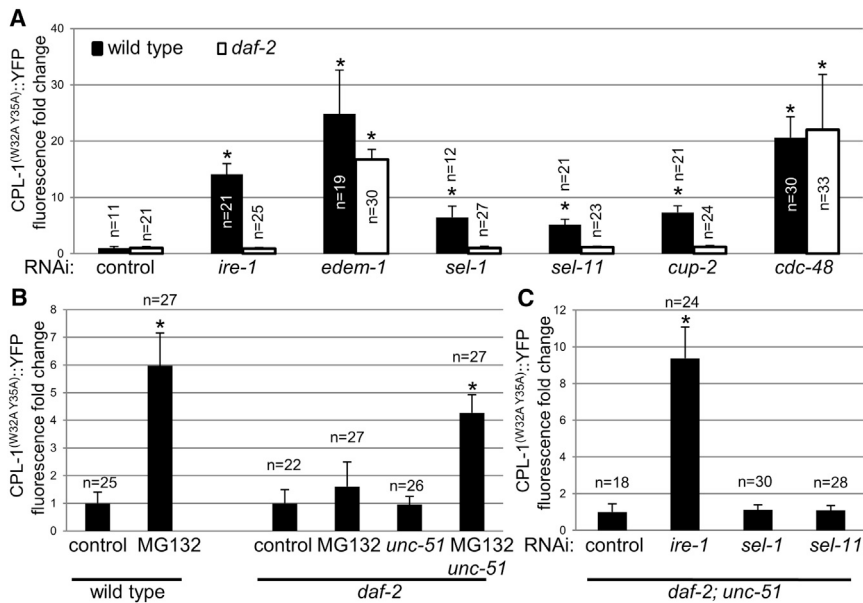
Figure 4. Misfolded Lumenal Proteins Can Be Degraded in a Proteasome-Dependent or a Lysosome-Dependent Manner in *daf-2* Mutants

(A) Fold change of mean fluorescence ± SEM of wild-type (black bars) or *daf-2* (white bars) CPL-1$^{(W32A\ Y35A)}$::YFP transgenic animals treated with the indicated RNAi. Student's t tests were calculated relative to the corresponding control RNAi.

(B and C) Fold change of mean fluorescence ± SEM of day 1 adults expressing CPL-1$^{(W32A\ Y35A)}$::YFP. Treatment with 40 μM proteasome inhibitor MG132 increased CPL-1$^{(W32A\ Y35A)}$::YFP fluorescence in *daf-2* mutants only in combination with an *unc-51* mutation. Student's t tests were calculated relative to DMSO-treated control animals (B). Proteasome-dependent ERAD in *daf-2; unc-51* double mutants is perturbed in *ire-1*-RNAi treated animals but not in *sel-1/sel-11* RNAi-treated animals (C). Student's t tests were calculated relative to control RNAi. Asterisks mark Student's t test values of $p < 0.0001$. "n" indicates number of animals analyzed. All results repeated at least three times independently.

See also Figure S3.

sel-11, and *cup-2* increased mutated CPL-1::YFP's fluorescence in wild-type animals but not in *daf-2* mutants (Figure 4A). The sustained ability to degrade aberrant lumenal proteins in the absence of these genes suggests that the *sel-11/sel-1* E3 ubiquitin ligase complex is not essential for the degradation of misfolded lumenal proteins in *daf-2* mutants.

A Proteasome-Mediated ERAD Pathway and an Autophagy-Mediated ERAD Pathway Act Side-by-Side in IIS Mutants

To examine whether the clearance of misfolded lumenal proteins is achieved by a proteasome-independent mechanism, the degradation of mutated CPL-1::YFP in *daf-2* mutants was examined upon inactivation of the proteasome. Treatment with the MG132 proteasome inhibitor blocked mutated CPL-1::YFP degradation in wild-type animals, but not in *daf-2* mutants (Figure 4B). Thus, in contrast to wild-type animals, misfolded lumenal proteins can be degraded by a proteasome-independent mechanism in *daf-2* mutants.

We further examined whether mutated CPL-1::YFP can be cleared by engulfment into autophagosomes. Blocking autophagosome formation using an *unc-51/ATG1* mutation did not abrogate the degradation of mutated-CPL-1::YFP in wild-type animals (Miedel et al., 2012) or in *daf-2* mutants (Figure 4B), consistent with the presence of a functional proteasome-mediated ERAD pathway in these animals. However, blocking the proteasome ERAD pathway using MG132 or using *ire-1* RNAi in the presence of an *unc-51* mutation increased the levels of mutated-CPL-1::YFP in *daf-2* mutants (Figures 4B and 4C). This suggests that an ERAD pathway, which clears lumenal aberrant proteins via autophagy, is present and active in *daf-2* mutants. Consistent with this, we observed an increase in autophagy as assessed by the number of LGG-1/LC3::GFP positive puncta in *ire-1; daf-2* double mutants compared to *ire-1* single mutants and wild-type animals (Figure S3); comparable to the increased levels observed in *daf-2* single mutants (Meléndez et al., 2003).

Does the autophagy-mediated ERAD pathway extract the proteins directly from the ER or does it still require retro-translocation to the cytosol? In support of the latter, we found that the cytosolic AAA-ATPase *cdc-48*, thought to give the force for the extraction of client misfolded proteins out of the ER (Rabinovich et al., 2002), is required for the clearance of mutated CPL-1::YFP both in wild-type animals and in *daf-2* mutants (Figure 4A). Thus, retro-translocation to the cytosol is an essential step in the degradation of aberrant lumenal proteins from the ER in *daf-2* mutants.

Interestingly, CPL-1::YFP fluorescence did not increase in *daf-2* mutants treated with *sel-1 or sel-11* RNAi, even when autophagosome formation was blocked (Figure 4C). Thus, in addition to enabling the clearance of lumenal proteins through autophagy, reducing IIS may also enable targeting and degradation of such proteins by the proteasome, bypassing the *sel-11/sel-1* E3 ubiquitin ligase complex. This suggests that reducing IIS enables the ubiquitination and the retro-translocation of mutated CPL-1::YFP independently of the *sel-11/sel-1* E3 ubiquitin ligase complex (see model Figure S6).

Nuclear DAF-16 Is Necessary and Sufficient for the Suppression of Many of the Phenotypes Associated with *ire-1* deficiency

Reducing IIS results in the translocation of the FOXO transcription factor DAF-16 into the nucleus (Lee et al., 2001; Lin et al., 2001). We found that reducing IIS no longer improved protein secretion in *daf-16; ire-1* double mutants, as reflected by its inability to increase DAF-28::GFP fluorescence in the body cavity of the animals and its inability to reduce DAF-28::GFP fluorescence in the intestinal-producing cells (Figures 5A and 5B). This implies that *daf-16* is required for improving DAF-28::GFP secretion by reducing IIS.

Next, we asked whether expression of a constitutively nuclear form of DAF-16 is sufficient for improving secretion in *ire-1* mutants. We used a characterized transgenic line expressing
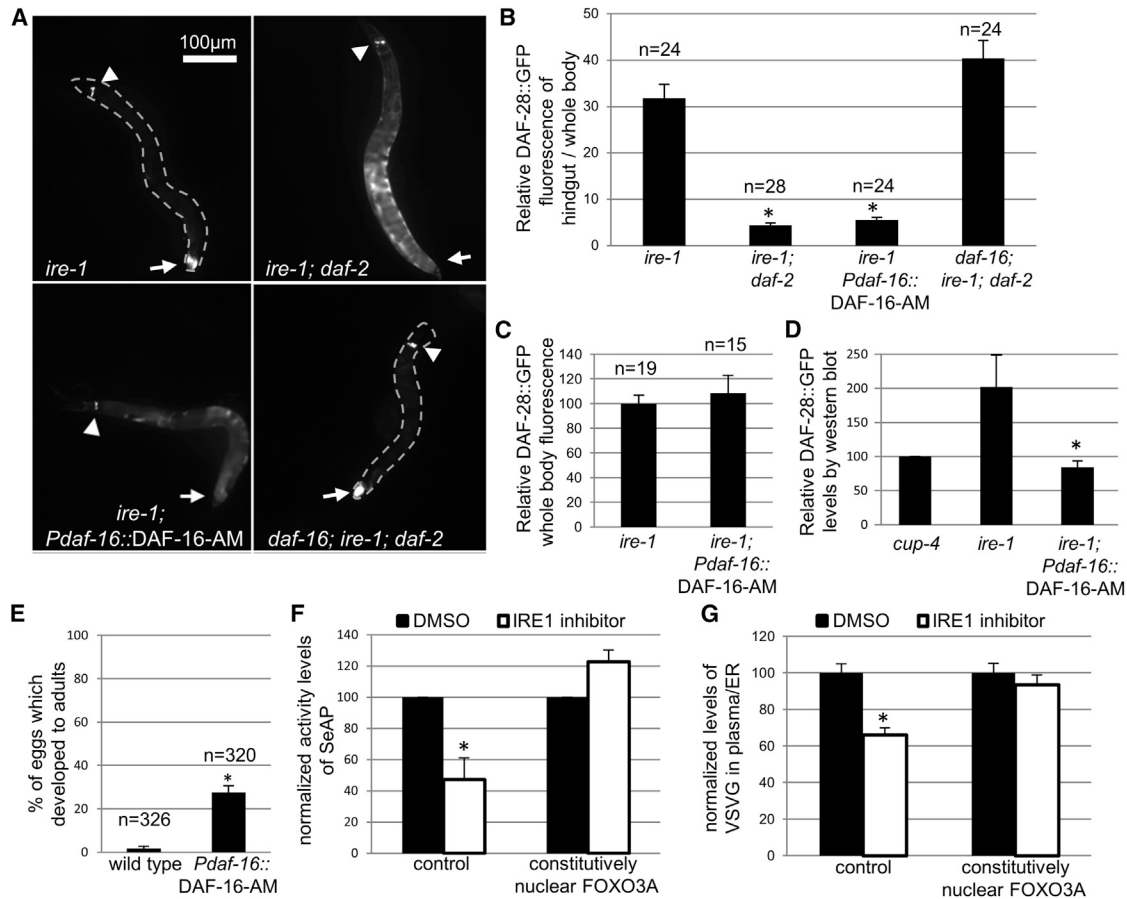
Figure 5. Nuclear *C. elegans* DAF-16 and Activated Mammalian FOXO3 Maintain ER Function and Secretory Protein Metabolism Independently of the IRE1 Pathway

(A) Representative fluorescence micrographs of day 3 animals harboring a DAF-28::GFP transgene. Full arrows mark hindgut. Arrowheads mark ASI/ASJ neurons.

(B) Mean fluorescence ± SEM of DAF-28::GFP in the hindgut producing cells relative to whole body fluorescence of the same animal. Asterisks mark Student's t test values of $p < 0.0001$ compared to *ire-1* single mutants. Similar results were obtained in three independent experiments.

(C) Expression of nuclear DAF-16-AM did not increase mean DAF-28::GFP whole body fluorescence in *ire-1*-deficient animals ($p = 0.28$). Similar results were obtained in three independent experiments.

(D) Expression of nuclear DAF-16-AM decreased mean DAF-28::GFP protein levels as assessed by western blotting in *ire-1*-deficient animals ($p < 0.0001$). DAF-28::GFP protein levels were normalized to tubulin levels in three independent biological experiments.

(E) Eggs of *Psod-3*::GFP expressing animals or animals expressing DAF-16[AM] and *Psod-3*::GFP were treated with 5 μg/ml tunicamycin. Percentage of animals that reached L4 or adult stage after 4 days ± SEM is shown.

(F) Treatment with the IRE1 inhibitor 4μ8C reduced the activity of a secreted alkaline phosphatase (SeAP) reporter in the cell culture medium of control HEK293 cells ($p < 0.01$). The activity of the secreted reporter SeAP was normalized to the activity of the cytosolic reporter Luciferase, driven by the same promoter. The activity of the SeAP reporter in the medium remained high even in the presence if the IRE1 inhibitor in cells expressing activated FOXO3 ($p = 0.12$).

(G) Treatment with the IRE1 inhibitor 4μ8C significantly increased the levels of a temperature-sensitive folding mutant of the vesicular stomatitis virus G protein (tsO45 VSVG) in the ER at the expense of its levels at the plasma membrane ($p < 0.0001$). Trafficking to the plasma membrane was not impaired by 4μ8C in cells coexpressing activated FOXO3 ($p = 0.23$). "n" indicates number of animals analyzed in (B), (C), and (E).

See also Figure S4.

an activated form of DAF-16, referred to as DAF-16[AM] (Lin et al., 2001). In DAF-16[AM], four potential AKT phosphorylation sites were replaced by alanine, mimicking a nonphosphorylated state of DAF-16, which forces its nuclear localization. Expression of DAF-16[AM] in *ire-1* mutants decreased the relative fluorescence of DAF-28::GFP in the intestinal cells without decreasing its overall fluorescence in the body cavity of the animals (Figures 5A–5C). This implies that nuclear DAF-16 is sufficient for improving DAF-28::GFP secretion in *ire-1* mutants, at least in

the intestine cells. Furthermore, although expression of DAF-16[AM] did not decrease DAF-28::GFP fluorescence in the whole animal (Figure 5C), it did decrease DAF-28::GFP protein levels measured by western blot (Figure 5D). This is consistent with the possibility that nuclear DAF-16 enables the clearance of misfolded DAF-28::GFP in *ire-1*-deficient animals. Accordingly, the constitutively nuclear DAF-16 transgene significantly increased the resistance of wild-type animals to tunicamycin (Figure 5E).
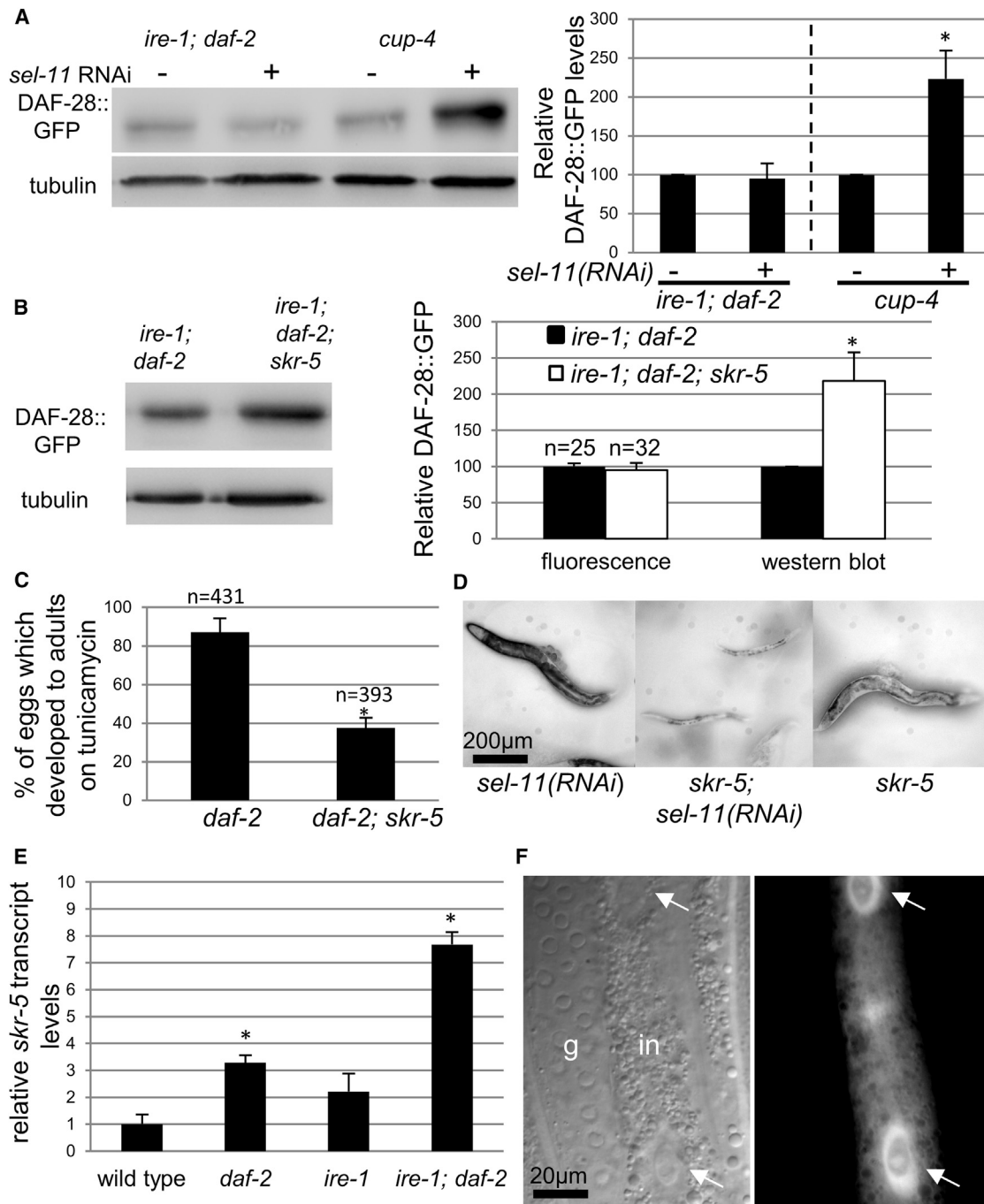
Figure 6. SKR-5 Localizes to the ER and Is Required for the Clearance of Misfolded Proteins in *ire-1; daf*-2 Mutants

(A) Representative western blot of DAF-28::GFP and tubulin of day 2 *cup-4* mutants and *ire-1; daf-2* double mutants expressing a DAF-28::GFP transgene treated with *sel-11* RNAi or control RNAi. Both strains are coelomocyte-defective. Bar graph presents the tubulin-normalized levels of DAF-28::GFP ± SEM in three independent biological experiments. Asterisks mark Student's t test values of $p < 0.01$ compared to control RNAi treatment.

(B) DAF-28::GFP levels were compared between *ire-1; daf-2* double mutants and *ire-1; daf-2*; *skr-5* triple mutants on day 2 of adulthood. Both strains are coelomocyte-defective. DAF-28::GFP and tubulin levels were assessed by western blot (left) and by fluorescence. Bar graph presents the normalized mean levels of DAF-28::GFP ± SEM as assessed by fluorescence or by western blot measurement. The experiment averages more than three independent biological repeats. "n" indicates number of animals analyzed.

(C) Eggs of the indicated genotypes were treated with 5 μg/ml tunicamycin. Percentage of eggs that developed into mature adults or L4 within 4 days ± SEM is shown. Each experiment was repeated independently with similar effects.

(D) *skr-5* mutants treated with control RNAi and wild-type animals treated with *sel-11* RNAi developed from eggs into adults within 3 days. *skr-5* mutants treated with *sel-11* RNAi did not complete their development into adults even after 6 days.

(legend continued on next page)

Activated FOXO3 Restores Secretory Trafficking in Human Cells with a Compromised IRE1 Pathway

Because DAF-16[AM] was sufficient for promoting the mainte-nance of ER homeostasis independently of *ire-1* in *C. elegans*, we wondered whether this pathway is conserved in higher or-ganisms as well. Thus, we examined whether expression of a constitutively nuclear form of the DAF-16 homolog FOXO3 could improve ER function in cells treated with an IRE1 inhibitor. To this end, a secreted alkaline phosphatase (SeAP) reporter gene was transfected into human embryonic kidney (HEK) 293 cells along with a control plasmid or a plasmid driving the expression of FOXO3A (an active FOXO3 mutant in which three potential AKT phosphorylation sites were replaced by alanine; Brunet et al., 2004). Treatment with the IRE1 inhibitor 4μ8C (Cross et al., 2012) significantly decreased the SeAP activity detected in the cell medium of the control-transfected cells, but remained high in the cell medium of cells cotransfected with FOXO3A (Figure 5F).

In addition, we followed the trafficking of a temperature-sensi-tive folding mutant of the vesicular stomatitis virus G protein (tsO45 VSVG) from the ER to the plasma membrane (Presley et al., 1997) in HEK293 cells. To this end, a GFP-tagged VSVG gene was transfected alone or together with a plasmid driving the expression of FOXO3A, and treated with the IRE1 inhibitor 4μ8C. VSVG levels at the ER and at the plasma membrane were determined after shifting cells to the permissive tempera-ture by quantifying the total fluorescence in two optical sections: one reporting on the nuclear rim and the ER ("middle"), and one focused on the adhering plasma membrane ("bottom"). We found that in cells without FOXO3A transfection, treatment with the IRE1 inhibitor significantly increased the levels of VSVG in the ER at the expense of its levels at the plasma membrane (Figure 5G). In contrast, trafficking of VSVG to the plasma mem-brane was not impaired by the IRE1 inhibitor in cells coexpress-ing FOXO3A (Figure 5G). Thus, the ability of nuclear DAF-16/ FOXO3A to maintain secretory protein metabolism indepen-dently of the IRE1 pathway is evolutionarily conserved, and ap-plies to a variety of secreted substrates (ssGFP, DAF-28::GFP, SeAP) and to transmembrane substrates (VSVG).

Several *daf-16*-target Genes Improve DAF-28::GFP Metabolism in *ire-1*-Deficient Animals

We explored whether known downstream targets of *daf-16* were important for the improved secretion in *ire-1* mutants expressing nuclear DAF-16. To this end, *ire-1* mutants expressing DAF-16[AM] and the DAF-28::GFP transgenes were treated with RNAi target-ing 263 genes known to be upregulated in *daf-2* mutants in *daf-16*-dependent manner (Murphy et al., 2003). We identified ten RNAi clones that hindered DAF-28::GFP secretion, resulting in an expression pattern similar to that of *ire-1* mutants (i.e., with a low level of fluorescent DAF-28::GFP in the body cavity and with high fluorescence in the intestinal cells that produce DAF-28::GFP; see Figure S4).

The effect of eight of these RNAi clones on DAF-28::GFP expression was validated (Figures S4B and S4C). These included a putative ER-Golgi transport-related gene (*dct-3*), a UDP-glucuronosyl transferase (*ugt-42*), a cytochrome P450 (*cyp-33C3*), a Skp1-like protein that acts as part of an SCF E3 ubiquitin ligase complex (*skr-5*), a putative gluthathione synthase (*gst-4*), a sorbitol dehydrogenase (*sodh-2*), a cathepsin protease (*cpz-2*), and *tps-1*, an enzyme required for the synthesis of treha-lose. Trehalose is known to stabilize protein folding (Kaushik and Bhat, 2003) and to increase autophagy (Sarkar et al., 2007). Given the improvement in ERAD function in *ire-1*-deficient ani-mals upon DAF-16 activation, and based on their potential involvement with the proteasome and autophagy degradation systems, we selected the *skr-5* and the *tps-1* genes for further validation.

Using quantitative RT-PCR, we confirmed that *skr-5* and *tps-1* transcript levels are increased when IIS is reduced, both in *ire-1(+)* and in *ire-1(−)* background (Figures 6E and S4E). In addition, we investigated how mutations in the *skr-5* and *tps-1* genes affected DAF-28::GFP levels in *ire-1; daf-2* double mutants. We found that in the absence of *skr-5*, DAF-28::GFP total protein levels increased (see western blot in Figure 6B), whereas its fluorescence levels remain unaltered (p = 0.47; Figure 6B). In contrast, the *tps-1* mutation modestly but consistently reduced DAF-28::GFP fluorescence in *ire-1; daf-2* double mutants by ∼25% (p < 0.01), without significantly affecting DAF-28::GFP protein levels as detected by western blotting (p = 0.17; Fig-ure S4D). Assuming that the fluorescence of misfolded DAF-28::GFP is compromised (Safra et al., 2013); this suggests that *skr-5* primarily promotes the degradation of misfolded proteins in *ire-1; daf-2* double mutants, whereas *tps-1* primarily improves protein folding presumably via trehalose production.

Unlike *sel-11*, *skr-5* Promotes Degradation of Misfolded DAF-28::GFP in *ire-1; daf-2* Double Mutants

How might *skr-5* promote the clearance of aberrant lumenal proteins in the ER? We generated transgenic animals expressing an SKR-5::GFP translational fusion. We detected SKR-5::GFP fluorescence both within the nucleus as well as in reticular-like structures characteristic to the ER in intestinal cells (Figure 6F). Furthermore, SKR-5::GFP colocalized with an intestinal ER marker using confocal microscopy, implying that SKR-5 can be recruited to the ER membrane (Figure S5).

We hypothesized that SKR-5 may act as an E3-ubiquitin ligase complex that ubiquitinates misfolded proteins that have been translocated from the ER to the cytosol by the quality control ma-chinery. Such a complex may be especially important in *ire-1*-deficient animals, whose *sel-11/sel-1* ERAD-related E3 ubiquitin ligase is not functional (Safra et al., 2013). Accordingly, we found a synthetic interaction between the *sel-11* and *skr-5* genes. Whereas *skr-5* single mutants and *sel-11* RNAi-treated animals developed from eggs to adults similarly to wild-type animals; *skr-5* mutants treated with *sel-11* RNAi remained arrested as

---

(E) Average relative mRNA levels ± SEM of *skr-5* measured by qRT-PCR in three independent experiments. Asterisks mark Student's t test values of p < 0.01 compared to the corresponding *daf-2(+)* animals.

(F) Representative Nomarski and fluorescence micrographs of an adult transgenic animal expressing *Pskr-5*::SKR-5::GFP. SKR-5::GFP expression was detected in intestine cells, both in the nuclei (indicated by arrows), as well as in reticular structures surrounding the nucleus and throughout the cell.

See Figure S5 for confocal images and colocalization with ER marker.
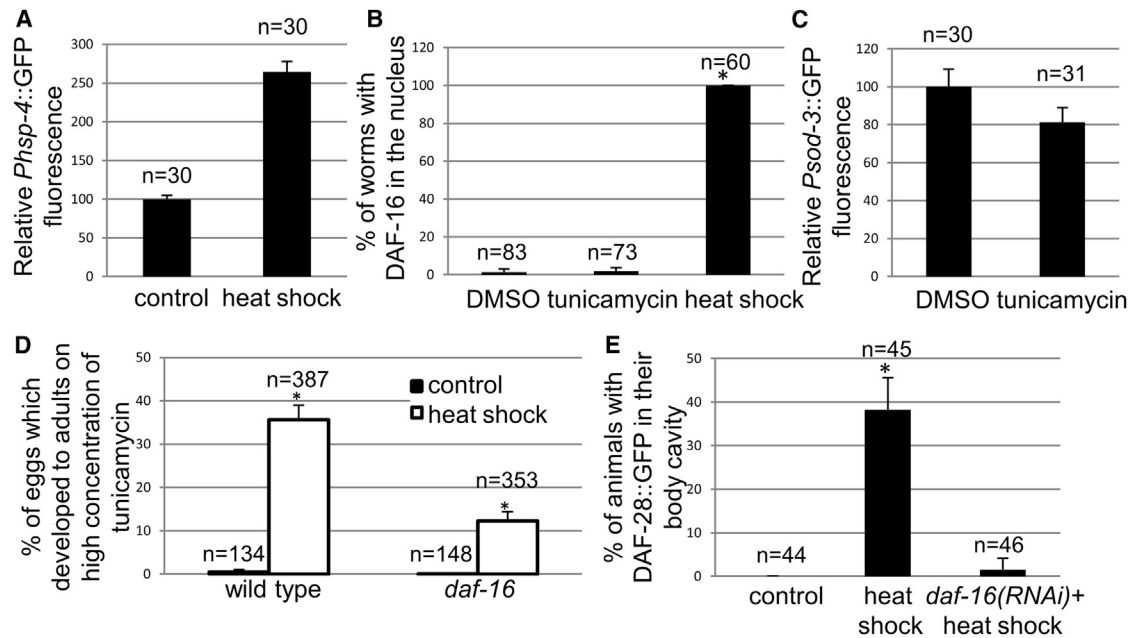
Figure 7. DAF-16 Promotes ER Homeostasis and ER Stress Resistance under Physiological Conditions

(A) Relative *Phsp-4*::GFP fluorescence levels measured 4 hr after exposing animals to 33°C for 1 hr.

(B) Percentage of animals with nuclear DAF-16::GFP after the indicated treatments. Three independent experiments were scored.

(C) Relative mean ratio ± SEM of *Psod-3*::GFP fluorescence of DMSO or tunicamycin-treated animals. *Psod-3* is a direct target of DAF-16.

(D) Wild-type or *daf-16(−)* eggs were treated with 5 μg/ml tunicamycin. Mean percentage of eggs that developed into mature L4 larvae or adults within 4 days ± SEM is shown. Animals were either untreated or heat shocked at 33°C for 1 hr, 1 day after they were laid.

(E) Percentage of *ire-1* mutants in which DAF-28::GFP is detected primarily in their body cavity instead of in their producing cells. Three independent experiments were scored. "n" indicates number of animals analyzed. Similar results were obtained in three independent experiments. Asterisks mark Student's t test values of p < 0.001 compared to control or to DMSO.

See Figure S6 for working model.

L2 larvae for at least 6 days (Figure 6D). Furthermore, unlike inactivation of *sel-11*, inactivation of *skr-5* significantly increased total protein levels of DAF-28::GFP in *ire-1; daf-2* double mutants (Figures 6A and 6B). Thus, whereas wild-type animals rely mainly on *sel-11* for the clearance of misfolded DAF-28::GFP, *ire-1; daf-2* double mutants rely on *skr-5* instead.

Whereas inactivation of both ERAD-related E3 ligase complexes was detrimental for the animals, we hypothesized that the combined activity of these complementary ERAD pathways may benefit the animals in times of stress. Accordingly, we found that *daf-2; skr-5* double mutants were significantly less resistant to tunicamycin compared to *daf-2* single mutants (Figure 6C). This supports the hypothesis that the combined activity of wild-type ERAD and *skr-5*-related ERAD benefits animals with reduced IIS. Furthermore, it is consistent with the increased levels of *skr-5* transcripts in *daf-2* mutants (Figure 6E).

Physiological Role of DAF-16 in Preserving ER Homeostasis

Does *daf-16* contribute to the maintenance of ER homeostasis only in *daf-2* mutants or does it act in a wider physiological context? First, we examined whether DAF-16 is directly activated in response to ER stress. We found that 24 hr exposure of adult animals to tunicamycin did not result in the translocation of DAF-16 to the nucleus, nor did it induce the expression of the DAF-16 target gene *sod-3* (Figures 7B and 7C). Thus, accumula-

tion of misfolded proteins in the ER does not directly activate DAF-16.

In nature, ER stress is not always induced in an isolated fashion and can also be induced as part of a wider cytotoxic response. For example, high temperatures activate the ER UPR (as detected by the induction of the *hsp-4* promoter-driven GFP, Figure 7A), the cytosolic heat-shock response, and the mitochondrial UPR. Thus, we examined whether heat-shock conditions, which promote DAF-16 nuclear translocation (Figure 7B), improve the animals' ability to deal with ER stress. We found that a short heat shock of tunicamycin-treated larva significantly increased the fraction of the animals that completed their development into adults in the presence of tunicamycin (Figure 7D). The improved resistance to tunicamycin upon heat shock treatment was, to a great extent, *daf-16* dependent (Figure 7D). Similarly, a short heat shock of day 1 *ire-1* mutants improved the secretion of DAF-28::GFP to the pseudocoelom in a *daf-16*-dependent manner (Figure 7E). Thus, activation of DAF-16 by natural stresses can actively promote ER homeostasis and function in wild-type and *ire-1*-deficient animals.

DISCUSSION

In *C. elegans*, reducing IIS promotes resistance to many stresses (Kenyon, 2010). Here, we deciphered how reducing IIS improves ER homeostasis and reduces sensitivity to ER stress. We

discovered that a parallel ER homeostasis-promoting system, that is independent of *xbp-1* and *ire-1*, exists in *daf-2* mutants. By handling part of the load of misfolded proteins in the ER, this ER homeostasis-promoting system can act together with the conserved UPR to improve protein folding and to clear and degrade terminally misfolded proteins from the ER. This reduces the basal load on the ER under normal growth conditions, as well as under ER stress conditions. Consequently, the *ire-1/xbp-1* pathway in *daf-2* mutants can be set at lower levels (Henis-Korenblit et al., 2010). Furthermore, the availability of two independent systems that promote ER homeostasis allows them to effectively deal with ER stress even when one of the pathways is compromised (for example upon loss of responsiveness of the *ire-1* UPR pathway, a phenomena associated with aging; Taylor and Dillin, 2013).

We find that conditions that promote the translocation of the DAF-16 transcription factor to the nucleus (Lin et al., 2001), promote the maintenance of ER homeostasis and function, independently of the canonical *ire-1/xbp-1* UPR pathway. Accordingly, expression of a constitutively nuclear form of DAF-16 is sufficient for improving ER homeostasis and function in *ire-1* mutants, as it is sufficient for increasing the number of LGG-1-positive foci (Jia et al., 2009). Nevertheless, as in the case of lifespan regulation (Lin et al., 2001), the improvement in ER homeostasis conferred by nuclear DAF-16 was not as high as that by the *daf-2* mutation. This may be due to insufficient expression levels of the nuclear DAF-16 transgene or due to additional molecular events associated with reduced IIS signaling that may also contribute to the ER stress resistance of *daf-2* mutants.

Although DAF-16 activation promotes ER homeostasis, perturbation of ER homeostasis per-se is not sufficient to activate this pathway. We hypothesize that the activation of DAF-16 by a variety of other cytotoxic stresses (as in the case of heat-shock and oxidative stresses), may have alleviated the evolutionary force to directly activate DAF-16 by disruption of ER homeostasis. This ER-independent activation of DAF-16 may set the ground for cross-stress hormesis, improving the animals' ability to deal with ER stress, even before ER homeostasis collapses. Furthermore, the regulation of ER homeostasis by DAF-16 activation may be tailored to meet broad cellular repair requirements associated with general cytotoxicity, which may be different from those required under isolated ER stress conditions.

How is ER homeostasis improved in IIS mutants? We discovered that this is achieved, at least in part, by facilitating the degradation and clearance of aberrant lumenal proteins from the ER. Unlike, the UPR in wild-type animals, which relies on the proteasome and on the *sel-1/sel-11* E3 ubiquitin ligase (Sasagawa et al., 2007); nuclear DAF-16 enables additional independent routes for the clearance of misfolded secretory proteins—via the proteasome and/or via autophagy (see model in Figure S6). Interestingly, in all pathways, retro-translocation to the cytosol is still required for the degradation and clearance of aberrant lumenal proteins from the ER in *daf-2* mutants. This suggests that client proteins are cleared from the cytosol and not directly from the ER. Consistent with this, we identified SKR-5 as required for the clearance of aberrant lumenal proteins in *ire-1; daf-2* mutants. Although SKR-5 is a cytosolic component

of a putative E3-ubiquitin ligase complex, it colocalizes with the ER. Thus, it is possible that an SKR-5 E3-ubiquitin ligase complex ubiquitinates ER client proteins upon their retro-translocation to the cytosol (see Figure S6). This is consistent with previous findings implicating FBS1/FBS2-containing SCF complexes in the ubiquitination of *N*-glycosylated proteins that have been translocated from the ER to the cytosol by the quality control machinery (Yoshida et al., 2002).

We identified additional *daf-16*-regulated genes whose inactivation compromised secretory protein metabolism upon activation of DAF-16. Interestingly, many of these genes are detoxification and cytoprotection-related genes. This implies that similarly to the ability to extend lifespan (Murphy et al., 2003; Shore and Ruvkun, 2013), the ability to overcome a compromised UPR relies on the integration and orchestration of a complex network of cytoprotective pathways. It will be interesting to decipher how each of these *daf-16* target genes promotes secretory protein metabolism. Because inactivation of the trehalose synthesizing enzyme *tps-1* primarily affected DAF-28::GFP folding rather than degradation, this indicates that reducing IIS improves multiple aspects of secretory protein metabolism.

ER homeostasis is essential for proper cellular function and its disruption contributes to heart disease, neurodegenerative disorders, diabetes, and more (Lin et al., 2008; Lindholm et al., 2006; Yoshida, 2007). Furthermore, many mutations in UPR genes result in pathologies: XBP1 and SEL1 heterozygous animals are resistant to insulin (Francisco et al., 2011; Ozcan et al., 2004). IRE1β and XBP-1 deficiencies in the intestine result in intestinal inflammation and sensitivity to colitis in mice (Bertolotti et al., 2001; Kaser et al., 2008). Several single nucleotide polymorphisms within the XBP1 gene locus are a major risk factor for Crohn's disease and ulcerative colitis (Kaser et al., 2008). This list of maladies associated with a dysfunctional UPR underscores the importance of signaling pathways, such as the IIS pathway, that can improve ER homeostasis even in the absence of a fully functional UPR. Importantly, we have demonstrated that activated FOXO3, similarly to its *C. elegans* homolog, protects ER function and maintains secretory protein metabolism independently of the IRE1 UPR pathway in mammalian cells. Because there is no sensor in the ER that activates DAF-16 in response to intrinsic ER stress, artificial activation of FOXO3 may be a promising therapeutic approach, paving the way for cures that will alleviate these diseases.

EXPERIMENTAL PROCEDURES

Strains
A list of strains used in this study is provided in the Supplemental Experimental Procedures.

Tunicamycin Resistance Assay
Tunicamycin resistance assays were performed as previously described (Henis-Korenblit et al., 2010) using plates containing low (1 µg/ml) or high (5 µg/ml) concentrations of tunicamycin (Sigma), as indicated.

Fluorescence Microscopy and Quantification
Animals were anaesthetized on 2% agarose pads containing 2 mM levamisol. Images were taken with a CCD digital camera using a Nikon 90i fluorescence microscope. Exposure time was kept constant through the experiment. NIS element software was used to quantify mean fluorescence intensity in the selected area.

xbp-1 Splicing and Quantitative RT-PCR

xbp-1 Splicing and quantitative RT-PCR were performed on day 1 animals as previously described (Safra et al., 2013). *xbp-1* PCR products were depicted on a 2% agarose gel and analyzed using ImageJ software. Real-time PCR was done using Maxima SYBR (Fermentas) in a Step one plus instrument. Transcript levels of *act-1* were used for normalization.

Western Blot

A similar number of animals were boiled in protein sample buffer containing 2% SDS. Anti-GFP (Roche, 1:1,000) and anti-tubulin (DHSB, 1:5,000) antibodies were used to detect proteins by western blotting.

RNAi Screen

Approximately 25 eggs of *ire-1* mutants expressing both DAF-28::GFP and nuclear DAF-16[AM] transgenes were placed on RNAi plates seeded with RNAi corresponding to 263 class I genes (Murphy et al., 2003). The fraction of animals whose DAF-28::GFP expression pattern was similar to that of *ire-1* mutants was scored. RNAi clone identity was verified by sequencing.

Confocal Microscopy

Confocal images were taken using an LSM 510 confocal scanning microscope (Carl Zeiss) with a 63 numerical aperture objective lens. Worms were mounted on 2% agarose pads containing 2 mM levamisol. Sections of 1.5 μm were taken. Colocalization was measured using ImageJ software.

Immunostaining

Synchronized day 2 adults were fixed in 4% paraformaldehyde, permeabilized with tween and β-mercaptoethanol overnight, and stained with anti-GFP (Roche, 1:1,000), and Cy3 conjugated secondary antibodies.

Autophagy Quantification

Autophagic events were observed using a fluorescent microscope Zeiss Imager Z1 and counted as in (Hansen et al., 2008). Briefly, *C. elegans* expressing GFP::LGG-1 (Meléndez et al., 2003) were placed on 2% agarose pads and foci were counted (using 1,000-fold magnification on a Zeiss Axioplan II microscope) in the seam cells of L3 larvae. Three independent biological repeats were carried out and the mean number of foci was averaged and plotted. Data were processed using PrismGraph.

Cell Culture

For the SeAP and luciferase assays, 8×10^4 HEK293 cells were seeded in a 24-well dish and transfected 24 hr later using Polyjet reagent (SignaGen Laboratories). Cells were transfected with a Promega pGL3-Control vector (for assessment of transfection efficiency) and a pSBC-2-SEAP vector (for assessment of protein production and secretion through the secretory pathway), with or without a Flag-FOXO3A-TM Addgene plasmid 8361 (to mimic reduction of IIS). SeAP activity in the medium was assessed with p-nitrophenyl phosphate substrate (Sigma) and luciferase activity was assessed using Promega dual luciferase kit.

For microscopy, HEK293 cells were seeded onto glass coverslips and cultured in Dulbecco's modified Eagle's medium (10% fetal calf serum, 1% pyruvate, 1% penicillin/streptomycin, and 1% L-glutamine). Cells were transfected 24 hr later with VSVG-GFP (Malchus and Weiss, 2010) with or without Flag-FOXO3A-TM (Addgene) using Lipofectamine 3000 (Life Technologies). After 24 hr at 39.5°C, part of the cells were treated with 50 μM IRE1-Inhibitor III, 4μ8C (Calbiochem, Merck Millipore), and kept for another 24 hr at 39.5°C. Cells with and without 4μ8C-treatment were shifted to 32°C for 60 min and then fixated with paraformaldehyde (4%). Fixed samples were mounted onto glass sample holders with Fluoromount-G (SouthernBiotech) and 25–50 cells were analyzed per treatment. Confocal imaging was done on a Leica SP5 confocal with a 63x/1.2NA water immersion objective and a 488 nm argon laser.

Statistical Analysis

All error bars show the SEM. The p values were calculated using the unpaired Student's t test, unless indicated otherwise.

REFERENCES

Bertolotti, A., Wang, X., Novoa, I., Jungreis, R., Schlessinger, K., Cho, J.H., West, A.B., and Ron, D. (2001). Increased sensitivity to dextran sodium sulfate colitis in IRE1beta-deficient mice. J. Clin. Invest. *107*, 585–593.

Brunet, A., Sweeney, L.B., Sturgill, J.F., Chua, K.F., Greer, P.L., Lin, Y., Tran, H., Ross, S.E., Mostoslavsky, R., Cohen, H.Y., et al. (2004). Stress-dependent regulation of FOXO transcription factors by the SIRT1 deacetylase. Science *303*, 2011–2015.

Calfon, M., Zeng, H., Urano, F., Till, J.H., Hubbard, S.R., Harding, H.P., Clark, S.G., and Ron, D. (2002). IRE1 couples endoplasmic reticulum load to secretory capacity by processing the XBP-1 mRNA. Nature *415*, 92–96.

Cross, B.C., Bond, P.J., Sadowski, P.G., Jha, B.K., Zak, J., Goodman, J.M., Silverman, R.H., Neubert, T.A., Baxendale, I.R., Ron, D., and Harding, H.P. (2012). The molecular basis for selective inhibition of unconventional mRNA splicing by an IRE1-binding small molecule. Proc. Natl. Acad. Sci. USA *109*, E869–E878.

Francisco, A.B., Singh, R., Sha, H., Yan, X., Qi, L., Lei, X., and Long, Q. (2011). Haploid insufficiency of suppressor enhancer Lin12 1-like (SEL1L) protein predisposes mice to high fat diet-induced hyperglycemia. J. Biol. Chem. *286*, 22275–22282.

Fujita, E., Kouroku, Y., Isoai, A., Kumagai, H., Misutani, A., Matsuda, C., Hayashi, Y.K., and Momoi, T. (2007). Two endoplasmic reticulum-associated degradation (ERAD) systems for the novel variant of the mutant dysferlin: ubiquitin/proteasome ERAD(I) and autophagy/lysosome ERAD(II). Hum. Mol. Genet. *16*, 618–629.

Hansen, M., Chandra, A., Mitic, L.L., Onken, B., Driscoll, M., and Kenyon, C. (2008). A role for autophagy in the extension of lifespan by dietary restriction in C. elegans. PLoS Genet. *4*, e24.

Henis-Korenblit, S., Zhang, P., Hansen, M., McCormick, M., Lee, S.J., Cary, M., and Kenyon, C. (2010). Insulin/IGF-1 signaling mutants reprogram ER stress response regulators to promote longevity. Proc. Natl. Acad. Sci. USA *107*, 9730–9735.

Jia, K., Thomas, C., Akbar, M., Sun, Q., Adams-Huet, B., Gilpin, C., and Levine, B. (2009). Autophagy genes protect against Salmonella typhimurium infection and mediate insulin signaling-regulated pathogen resistance. Proc. Natl. Acad. Sci. USA *106*, 14564–14569.

Kaser, A., Lee, A.H., Franke, A., Glickman, J.N., Zeissig, S., Tilg, H., Nieuwenhuis, E.E., Higgins, D.E., Schreiber, S., Glimcher, L.H., and Blumberg, R.S. (2008). XBP1 links ER stress to intestinal inflammation and confers genetic risk for human inflammatory bowel disease. Cell *134*, 743–756.

Kaushik, J.K., and Bhat, R. (2003). Why is trehalose an exceptional protein stabilizer? An analysis of the thermal stability of proteins in the presence of the compatible osmolyte trehalose. J. Biol. Chem. *278*, 26458–26465.

Kenyon, C.J. (2010). The genetics of ageing. Nature *464*, 504–512.

Kikkert, M., Doolman, R., Dai, M., Avner, R., Hassink, G., van Voorden, S., Thanedar, S., Roitelman, J., Chau, V., and Wiertz, E. (2004). Human HRD1 is an E3 ubiquitin ligase involved in degradation of proteins from the endoplasmic reticulum. J. Biol. Chem. *279*, 3525–3534.

Knop, M., Finger, A., Braun, T., Hellmuth, K., and Wolf, D.H. (1996). Der1, a novel protein specifically required for endoplasmic reticulum degradation in yeast. EMBO J. *15*, 753–763.

Lee, R.Y., Hench, J., and Ruvkun, G. (2001). Regulation of C. elegans DAF-16 and its human ortholog FKHRL1 by the daf-2 insulin-like signaling pathway. Curr. Biol. *11*, 1950–1957.

Lin, K., Hsin, H., Libina, N., and Kenyon, C. (2001). Regulation of the Caenorhabditis elegans longevity protein DAF-16 by insulin/IGF-1 and germline signaling. Nat. Genet. *28*, 139–145.

Lin, J.H., Walter, P., and Yen, T.S. (2008). Endoplasmic reticulum stress in disease pathogenesis. Annu. Rev. Pathol. *3*, 399–425.

Lindholm, D., Wootz, H., and Korhonen, L. (2006). ER stress and neurodegenerative diseases. Cell Death Differ. *13*, 385–392.

Malchus, N., and Weiss, M. (2010). Anomalous diffusion reports on the interaction of misfolded proteins with the quality control machinery in the endoplasmic reticulum. Biophys. J. *99*, 1321–1328.

Mehnert, M., Sommer, T., and Jarosch, E. (2014). Der1 promotes movement of misfolded proteins through the endoplasmic reticulum membrane. Nat. Cell Biol. *16*, 77–86.

Meléndez, A., Tallóczy, Z., Seaman, M., Eskelinen, E.L., Hall, D.H., and Levine, B. (2003). Autophagy genes are essential for dauer development and life-span extension in C. elegans. Science *301*, 1387–1391.

Miedel, M.T., Graf, N.J., Stephen, K.E., Long, O.S., Pak, S.C., Perlmutter, D.H., Silverman, G.A., and Luke, C.J. (2012). A pro-cathepsin L mutant is a luminal substrate for endoplasmic-reticulum-associated degradation in C. elegans. PLoS ONE *7*, e40145.

Molinari, M., Calanca, V., Galli, C., Lucca, P., and Paganetti, P. (2003). Role of EDEM in the release of misfolded glycoproteins from the calnexin cycle. Science *299*, 1397–1400.

Murphy, C.T., McCarroll, S.A., Bargmann, C.I., Fraser, A., Kamath, R.S., Ahringer, J., Li, H., and Kenyon, C. (2003). Genes that act downstream of DAF-16 to influence the lifespan of Caenorhabditis elegans. Nature *424*, 277–283.

Oh, S.W., Mukhopadhyay, A., Svrzikapa, N., Jiang, F., Davis, R.J., and Tissenbaum, H.A. (2005). JNK regulates lifespan in Caenorhabditis elegans by modulating nuclear translocation of forkhead transcription factor/DAF-16. Proc. Natl. Acad. Sci. USA *102*, 4494–4499.

Ozcan, U., Cao, Q., Yilmaz, E., Lee, A.H., Iwakoshi, N.N., Ozdelen, E., Tuncman, G., Görgün, C., Glimcher, L.H., and Hotamisligil, G.S. (2004). Endoplasmic reticulum stress links obesity, insulin action, and type 2 diabetes. Science *306*, 457–461.

Patton, A., Knuth, S., Schaheen, B., Dang, H., Greenwald, I., and Fares, H. (2005). Endocytosis function of a ligand-gated ion channel homolog in Caenorhabditis elegans. Curr. Biol. *15*, 1045–1050.

Presley, J.F., Cole, N.B., Schroer, T.A., Hirschberg, K., Zaal, K.J., and Lippincott-Schwartz, J. (1997). ER-to-Golgi transport visualized in living cells. Nature *389*, 81–85.

Rabinovich, E., Kerem, A., Fröhlich, K.U., Diamant, N., and Bar-Nun, S. (2002). AAA-ATPase p97/Cdc48p, a cytosolic chaperone required for endoplasmic reticulum-associated protein degradation. Mol. Cell. Biol. *22*, 626–634.

Richardson, C.E., Kinkel, S., and Kim, D.H. (2011). Physiological IRE-1-XBP-1 and PEK-1 signaling in Caenorhabditis elegans larval development and immunity. PLoS Genet. *7*, e1002391.

Ron, D., and Walter, P. (2007). Signal integration in the endoplasmic reticulum unfolded protein response. Nat. Rev. Mol. Cell Biol. *8*, 519–529.

Safra, M., and Henis-Korenblit, S. (2014). A new tool in C. elegans reveals changes in secretory protein metabolism in ire-1-deficient animals. Worm *3*, e27733.

Safra, M., Ben-Hamo, S., Kenyon, C., and Henis-Korenblit, S. (2013). The ire-1 ER stress-response pathway is required for normal secretory-protein metabolism in C. elegans. J. Cell Sci. *126*, 4136–4146.

Sarkar, S., Davies, J.E., Huang, Z., Tunnacliffe, A., and Rubinsztein, D.C. (2007). Trehalose, a novel mTOR-independent autophagy enhancer, accelerates the clearance of mutant huntingtin and α-synuclein. J. Biol. Chem. *282*, 5641–5652.

Sasagawa, Y., Yamanaka, K., and Ogura, T. (2007). ER E3 ubiquitin ligase HRD-1 and its specific partner chaperone BiP play important roles in ERAD and developmental growth in Caenorhabditis elegans. Genes Cells *12*, 1063–1073.

Shen, X., Ellis, R.E., Lee, K., Liu, C.Y., Yang, K., Solomon, A., Yoshida, H., Morimoto, R., Kurnit, D.M., Mori, K., and Kaufman, R.J. (2001). Complementary signaling pathways regulate the unfolded protein response and are required for C. elegans development. Cell *107*, 893–903.

Shen, X., Ellis, R.E., Sakaki, K., and Kaufman, R.J. (2005). Genetic interactions due to constitutive and inducible gene regulation mediated by the unfolded protein response in C. elegans. PLoS Genet. *1*, e37.

Shore, D.E., and Ruvkun, G. (2013). A cytoprotective perspective on longevity regulation. Trends Cell Biol. *23*, 409–420.

Smith, M.H., Ploegh, H.L., and Weissman, J.S. (2011). Road to ruin: targeting proteins for degradation in the endoplasmic reticulum. Science *334*, 1086–1090.

Taylor, R.C., and Dillin, A. (2013). XBP-1 is a cell-nonautonomous regulator of stress resistance and longevity. Cell *153*, 1435–1447.

Urano, F., Wang, X., Bertolotti, A., Zhang, Y., Chung, P., Harding, H.P., and Ron, D. (2000). Coupling of stress in the ER to activation of JNK protein kinases by transmembrane protein kinase IRE1. Science *287*, 664–666.

Urano, F., Calfon, M., Yoneda, T., Yun, C., Kiraly, M., Clark, S.G., and Ron, D. (2002). A survival pathway for Caenorhabditis elegans with a blocked unfolded protein response. J. Cell Biol. *158*, 639–646.

Yoshida, H. (2007). ER stress and diseases. FEBS J. *274*, 630–658.

Yoshida, Y., Chiba, T., Tokunaga, F., Kawasaki, H., Iwai, K., Suzuki, T., Ito, Y., Matsuoka, K., Yoshida, M., Tanaka, K., and Tai, T. (2002). E3 ubiquitin ligase that recognizes sugar chains. Nature *418*, 438–442.